Journal of Alloys and Compounds 911 (2022) 165103

Contents lists available at ScienceDirect

Journal of Alloys and Compounds

journal homepage: www.elsevier.com/locate/jalcom

Tuning deformation mechanisms of face-centered-cubic high-entropy alloys via boron doping

Haitao Zhang[a], Chenglin Wang[a], Shuyan Shi[a,*], Tingju Li[a], Longjiang Zou[a], Yiping Lu[a,b,**], Peter K. Liaw[c]

[a] Engineering Research Center of High entropy Alloy Materials (Liaoning Province), School of Materials Science and Engineering, Dalian University of Technology, Dalian 116024, China
[b] Key Laboratory of Solidification Control and Digital Preparation Technology (Liaoning Province), School of Materials Science and Engineering, Dalian University of Technology, Dalian 116024, China
[c] Department of Materials Science and Engineering, The University of Tennessee, Knoxville, TN 37996, USA

ARTICLE INFO

Article history:
Received 17 January 2022
Received in revised form 10 April 2022
Accepted 17 April 2022
Available online 20 April 2022

Keywords:
High entropy alloys
Mechanical properties
Boron doping
Deformation mechanism
Dislocation

ABSTRACT

Face-centered-cubic (FCC) high-entropy alloys (HEAs) can be strengthened through boron doping. However, the existing form of boron and its effect on the deformation mechanism of FCC HEAs have been rarely reported. The present work demonstrates for the first time the effect of the interstitial boron and boron-rich precipitate on the deformation mechanisms of the FCC (CoCrFeNi) HEAs. The dominant deformation mechanism of CoCrFeNi HEAs is dislocation slip, whereas the interstitial boron atoms dissolved in the matrix, thereby reducing the stacking fault energy (SFE) and transforming the dominant deformation mechanism to deformation twins. The loss of Cr from the matrix after boride formation increased the SFE, which led to transforming the dominant deformation mechanism from deformation twins to dislocation slip. Based on the results, we firstly propose to tune the deformation mechanism of FCC HEAs via boron doping, which provide a new strategy for designing and optimizing the HEAs.

1. Introduction

High-entropy alloys (HEAs) composed of multiple elements (≥ 4) break the shackles of the traditional alloy-design ideas [1,2]. Due to the high configurational mixing entropy, HEAs generally have a single crystal structure, such as face-centered-cubic (FCC) or body-centered-cubic (BCC) instead of complex intermetallic compounds [3–5]. Usually, FCC-structured HEAs, such as the CoCrFeNi HEAs, with a simple FCC phase have excellent ductility, but low strength that limits their industrial applications [6]. Many methods have been applied to improve the yield strengths of the FCC-structured HEAs, such as interstitial solid solution strengthening, precipitation strengthening, and grain-refinement strengthening [7–10]. Adding a nonmetal element (such as carbon, oxygen or nitrogen) to the HEAs can simultaneously satisfy these strengthening methods [11–15]. For instance, Wang et al. showed that the addition of 1.1 at. percent (at%) carbon to a single-phase FCC Fe40.4Ni11.3Mn34.8Al7.5Cr6 HEA, not only markedly increased the yield strength, but also led to a 25% increase in the elongation to fracture [16]. Another study demonstrated that adding 0.5 at% nitrogen to the NiCoCr medium-entropy alloy increased the yield strength without losing the ductility [17]. In contrast, boron preferentially precipitated on the grain boundary. The boron segregation is driven by the reduction of Gibbs free energy, and the bond property and load-bearing capacity of the alloy are improved by the interfacial strengthening [18–20].

Boron as an ideal dopant can significantly improve the mechanical properties of traditional alloys and HEAs. By adding boron to Ni_3Al, the yield strength can be increased by 242–387 MPa per atomic percent, and its ductility can also be significantly improved [20]. Ultra-high strength and excellent ductility can be obtained by adding boron to an equiatomic Fe20Mn20Cr20Co20Ni20 HEA and a non-equiatomic Fe40Mn40Cr10Co10 HEA [21].

The aforementioned research results demonstrate that it is promising to improve the mechanical properties of the HEAs by interstitial strengthening, but solubility of boron is quite limited in the HEAs. When boron is heavily doped, borides are often formed, which may change the alloy composition of the HEAs [22]. In HEAs, the deformation mechanism mainly depends on the stacking fault

* Corresponding author.
** Corresponding author at: Engineering Research Center of High entropy Alloy Materials (Liaoning Province), School of Materials Science and Engineering, Dalian University of Technology, Dalian 116024, China.
E-mail addresses: ssy@dlut.edu.cn (S. Shi), luyiping@dlut.edu.cn (Y. Lu).

https://doi.org/10.1016/j.jallcom.2022.165103
0925-8388/

energy (SFE), and one of the main factors affecting SFE is attributed to the alloy composition [23]. Consequently, the formation of borides may change the deformation mechanism of the HEAs, thereby influencing their mechanical properties. At present, researchers are still limited to the study of the effect of interstitial solution of boron on the deformation mechanism of HEA, but the effect of borides on the deformation mechanism has not been involved. It is of great significance to understand the effect of boron on the SFE of HEAs, which can reveal the deeper reasons for the change of deformation mechanism. Thus, the relationship between boron and the deformation mechanism is established.

In the present study, the CoCrFeNiB0.3 HEA was prepared to realize the coexistence of the interstitial solid solution and precipitation of boron atoms. The existing form of boron and its effect on the deformation mechanism of the CoCeFeNi HEA was systematically investigated by micro-cantilever tests [24–28]. In order to reveal the effect of boron on the deformation mechanism, stacking fault (SF) widths were measured to characterize the SFE [29]. According to the research results, the deformation mechanism of CoCrFeNi HEAs could be tuned via boron doping, which might provide a new insight for designing and optimizing HEAs through the interstitial atoms.

2. Materials and methods

The CoCrFeNi and CoCrFeNiB0.3 HEAs were prepared by vacuum arc melting. Electron probe microanalysis (JXA-8530 F PLUS) with a wavelength-dispersive spectrometer (WDS) was used to observe the microstructures and identify the elemental distributions of the CoCrFeNi and CoCrFeNiB0.3 HEAs. To ensure the data accuracy, the corresponding area of each sample was tested seven times to calculate the average value.

To investigate the effect of existing form of boron, such as the interstitial solution and precipitation on the strengthening mechanism and deformation mechanism, micro-cantilever beams were fabricated from the matrix of the CoCrFeNi HEA and the CoCrFeNiB0.3 matrix and dendrite, using the focused ion beam (FIB) instrument (Helios GX40). The lengths (L_0) of all cantilever beams were 12 μm and the widths (W) were 2 μm, with an equilateral triangular cross-section. To avoid the indenter offset during loading, a 1.5 × 1.2 × 0.5 μm pit was fabricated at the lower pressing end of the sample to restrain the indenter. The micro-bending tests were performed on a nanoindentation system (Hysitron TI 950). The deflection rate at the free end was 10 nm/s, and the downward displacement was 2 μm. Subsequently, the TEM samples were fabricated from the root of the deformed micro-cantilevers by the FIB instrument. The microstructure was characterized, employing TEM (JSM-F200), operating at 200 kV.

3. Result and discussion

The CoCrFeNi HEA only contains a single phase (Fig. 1a). The experimental result was in good agreement with the previous reports [30]. After adding boron, borides were formed in the CoCrFeNiB0.3 HEA (Fig. 1b). As shown in Table 1, the content of boron was 0.3104 at% in the CoCrFeNiB0.3 matrix (a red rectangular box), which indicates that boron was dissolved in the form of interstitial atoms. By contrast, there was almost no presence of boron in the matrix of the CoCrFeNiB0.3 dendrite (a blue rectangular box). Fig. 1(c-f) show that the matrix is the FCC phase, and the boride is Cr_2B, which was observed by transmission electron microscopy (JSM-F200, TEM) [31].

Fig. 2(a) is the representative SEM image of a micro-cantilever beam with an equilateral triangular cross section. As shown in Fig. 1(a-b), the green, red, and blue rectangular boxes represent the selected sample positions corresponding to the sample that does not contain boron (green), contains the boron in forms of the interstitial solid solution (red) and precipitates (blue), respectively. The corresponding load-displacement curves were obtained as shown in Fig. 2(b). The yield strengths of the micro-cantilever beams were calculated from the load versus displacement data, using standard slender beam equations [Fig. 2(b), see the Supplementary Materials for more details]. The yield strengths of the CoCrFeNi HEA, CoCrFeNiB0.3 matrix and dendrite were 230, 330, and 405 MPa, respectively. For the CoCrFeNi HEA, the obvious fluctuation can be found in the curve, which could be attributed to the dislocation slip [32]. By contrast, the fluctuations of curves corresponding to the CoCrFeNiB0.3 matrix and dendrite were very slight, because boron atoms pin the dislocation, and the precipitates hinder the dislocation

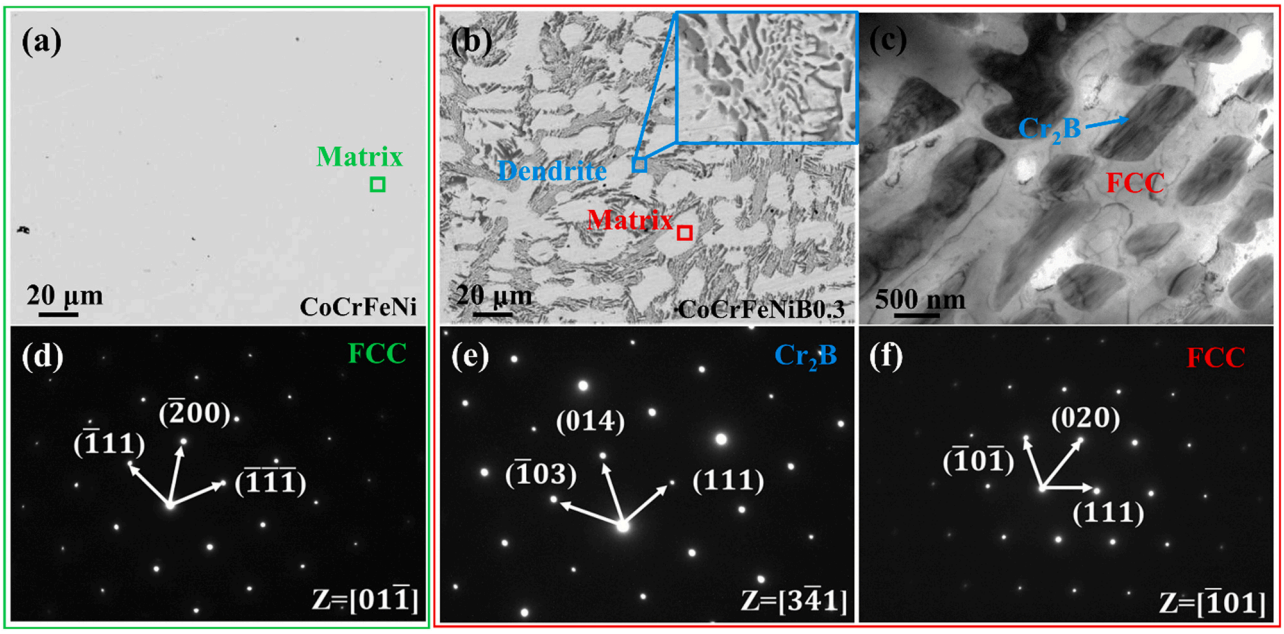

Fig. 1. (a) and (b) Backscattered electron images of the CoCrFeNi HEA and CoCrFeNiB0.3 HEA. (c) TEM image of the CoCrFeNiB0.3 HEA. (d-f) The corresponding selected area electron diffraction patterns of FCC and Cr_2B in CoCrFeNi and CoCrFeNiB0.3 HEAs.

Table 1
Chemical compositions (at%) of different regions in CoCrFeNi and CoCrFeNiB0.3 HEAs.

Alloys	Regions	Co	Cr	Fe	Ni	B
CoCrFeNi HEA	Matrix	25.3732	24.5609	25.7164	24.3494	0
CoCrFeNiB0.3	Matrix	25.0057	22.1752	26.8200	25.5939	0.3104
HEA	Matrix of Dendrite	25.1337	24.3881	26.775	25.4661	0.073

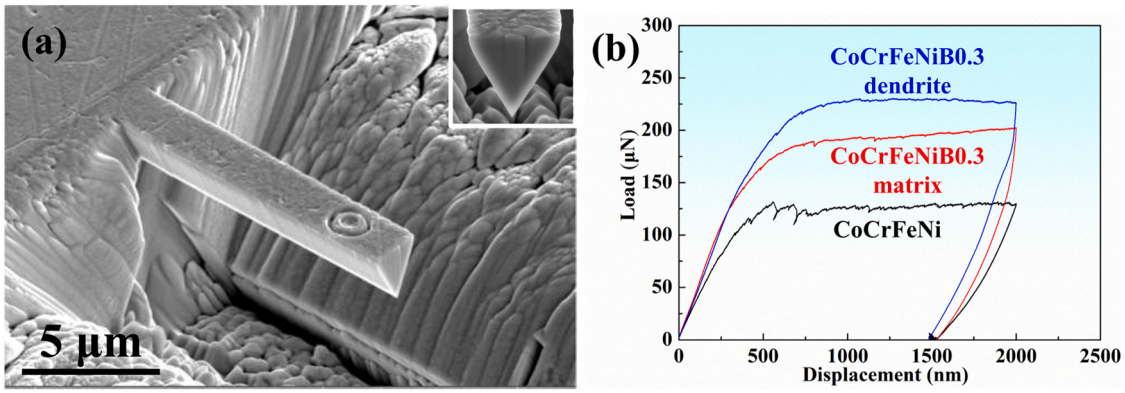

Fig. 2. (a) Representative SEM image of a micro-cantilever beam with an equilateral triangular cross section. (b) Load-displacement curves of micro-cantilever beams of CoCrFeNi and CoCrFeNiB0.3 HEAs.

movement. Subsequently, the strengthening mechanism of CoCrFeNiB0.3 HEA, including the precipitation strengthening and solid solution strengthening was investigated. Compared with CoCrFeNi HEA, the yield strength of CoCrFeNiB0.3 matrix and dendrite were enhanced by the interstitial solid solution strengthening and precipitation strengthening, and the corresponding values were 100 MPa and 175 MPa, respectively. Since the micro-cantilever beam was obtained on one grain, the effect of grain size on strength was not discussed in this study.

Fig. 3 shows the deformation mechanisms of the CoCrFeNi HEA during the micro-cantilever-bending tests. A large number of dislocation lines were seen in the deformed CoCrFeNi HEA [Fig. 3(a)]. A small number of deformation twins were activated in some areas, as presented in Fig. 3(b). The experimental results were consistent with those of other FCC HEAs [33]. Fig. 3(c) shows the HRTEM and FFT patterns corresponding to the rectangular box in Fig. 3(b). The dark fringes were identified as the deformation twins. Fig. 3(d) indicates that the deformation twins occurred on the $(1\bar{1}1)$ plane, which were $(1\bar{1}1)[21\bar{1}]$ type. In FCC metals with the low SFE, the dissociation of a 1/2 < 110 > perfect dislocation into a pair of 1/6 < 112 > Shockley partial dislocation in the {111} close-packed plane results in an intrinsic stacking fault. This process was repeated on successive {111} planes, thus forming a twin structure [34]. However, compared with the dislocations, the content of deformation twins and SFs was very small. Thus, the dislocation slip is the dominant deformation mechanism of the CoCrFeNi HEA.

Fig. 4 shows the deformation mechanisms of the CoCrFeNiB0.3 matrix and dendrite during the micro-cantilever bending tests. After adding boron, the deformation mechanism of the CoCrFeNiB0.3 HEA is obviously different from that of the CoCrFeNi HEA. Fig. 4(a) and the inset show that numerous deformation twins were activated in the CoCrFeNiB0.3 matrix, which were much larger than that in the CoCrFeNi HEA (Fig. 3). Fig. 4(b) is an enlarged image corresponding to the red rectangular box in Fig. 4(a). The interaction between the deformation twins and SFs can also be found in Fig. 4(b). After adding boron to the CoCrFeNi HEA, the dominant deformation mechanism of the CoCrFeNiB0.3 matrix was transformed from the dislocation slip to deformation twins.

Fig. 4(c-d) show the deformation mechanisms of the CoCrFeNiB0.3 dendrite, and some borides can be observed in Fig. 4(c). The microstructure near the borides was further magnified (to better investigate the mechanism), as demonstrated in Fig. 4(d). The dislocation accumulation could be observed in the vicinity of borides, indicating that the dislocation movement was hindered by borides. Thus, the dominant deformation mechanism of the CoCrFeNiB0.3 dendrite mechanism is the dislocation slip.

The results indicate that adding boron to the CoCrFeNi HEA significantly affected the deformation mechanism, which can be attributed to the change of the SFE. To characterize the SFE of HEAs, we measured the width of SF in the CoCrFeNi HEA, CoCrFeNiB0.3 matrix and dendrite by HRTEM. Fig. 5 shows the typical microstructure of the SF formed by the dissociation of a full dislocation. The type of full dislocations was determined by drawing the Burgers circuits around entire SFs. The close failure of the Burgers circuit was measured to be $a/4[\bar{2}11]$, which presented the projection vector of the Burgers vector of the full dislocation to form the SF by dissociation [29]. The relationship between the SFE and SF width can be expressed as follows [35]:

$$\gamma = \frac{G\vec{b_1}\cdot\vec{b_2}}{2\pi d}$$

where G is the shear modulus, γ is the stacking fault energy, b_1 and b_2 are Burgers vectors of two partial dislocations, d is the width of SF. According to the formula, the SF width is inversely proportional to the SFE. The corresponding SF widths of the CoCrFeNi HEA and the CoCrFeNiB0.3 matrix and dendrite were approximately 4.3 nm, 6.9 nm, and 1.5 nm, respectively. Thus, the order of SFE was as follows: CoCrFeNiB0.3 dendrite > CoCrFeNi HEA > CoCrFeNiB0.3 matrix.

For the CoCrFeNi HEA, numerous dislocation lines were generated after deformation, indicating that the dominant deformation mechanism was dislocation slip [Fig. 3(a)]. Since the CoCrFeNi HEA with an FCC structure had a low SFE, a small number of deformation twins were activated, as shown in Fig. 3(b) and (c) [36]. A basic principle of this behavior is that the perfect dislocations are dissociated into the Shockley partials and formed SFs. Then, the SFs formed in the same way on same adjacent slip planes were dynamically superimposed to the previous SFs one by one. Eventually, the SFs were superimposed to form the deformation twins. Similar

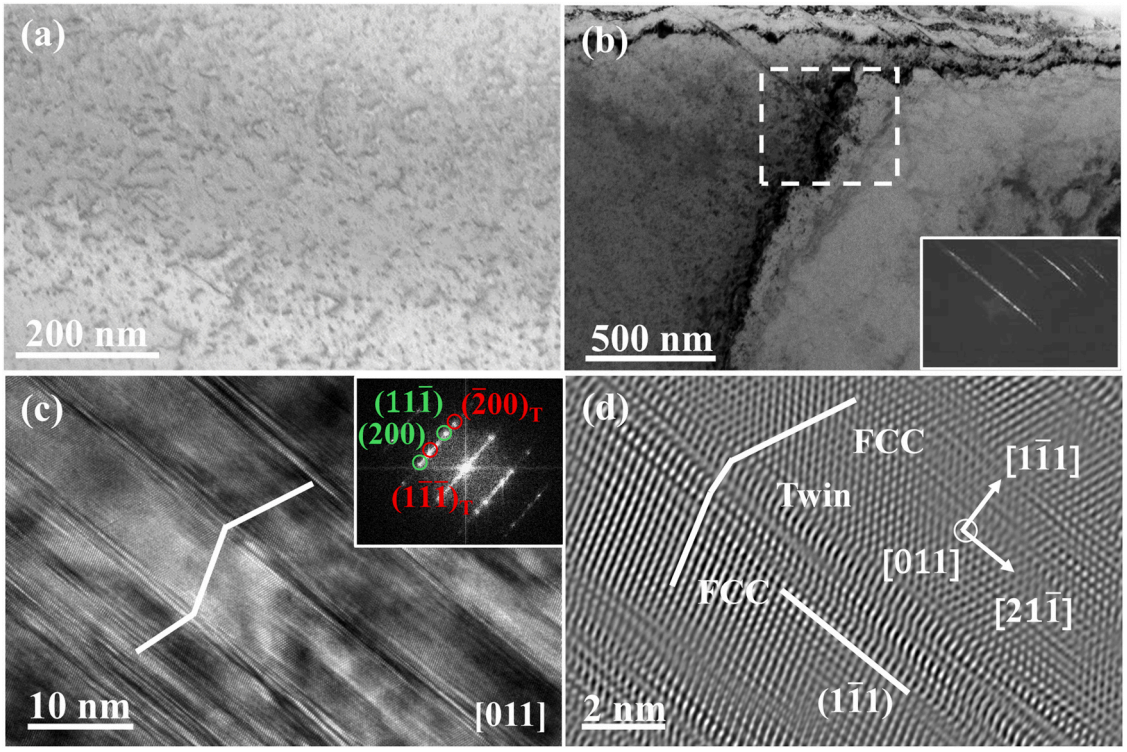

Fig. 3. Deformation mechanisms of the CoCrFeNi HEA during the micro-cantilever bending tests. (a) Dislocation structures after deformation. (b) Bright field image and corresponding dark-field image of the deformation twins. (c) and (d) Representative high resolution transmission electron microscopy (HRTEM) and inverse fast Fourier transform (IFFT) images of the deformation twins, (the inset is the corresponding fast Fourier transform (FFT)).

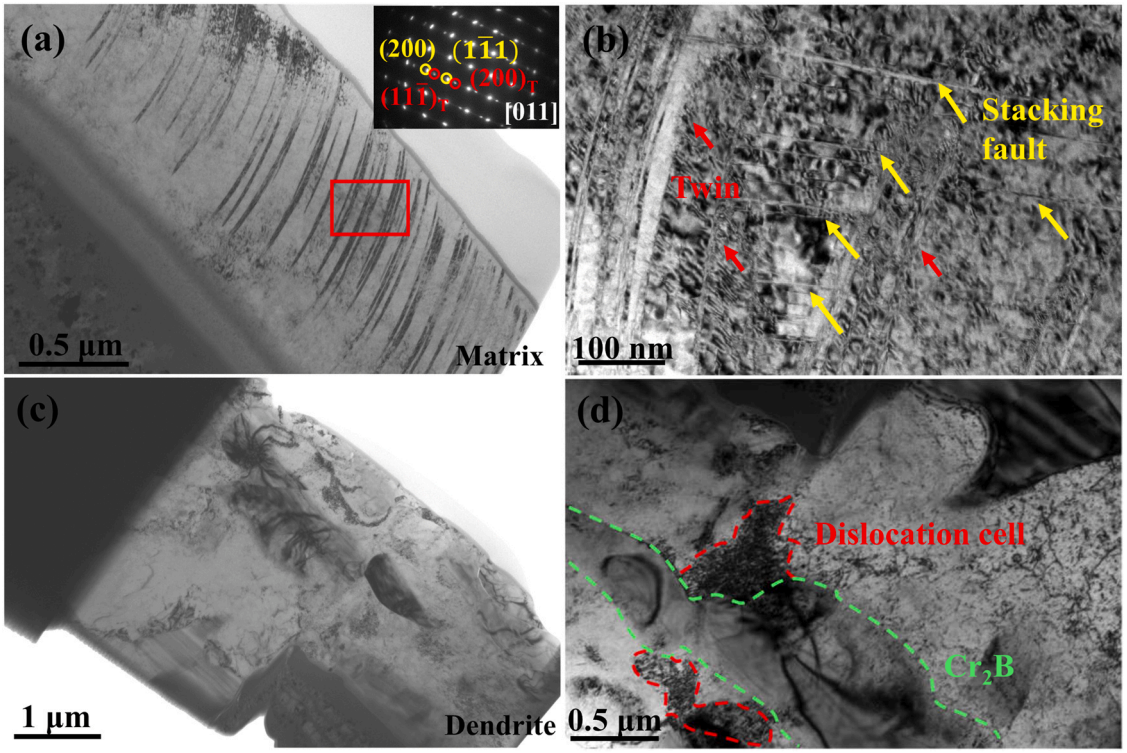

Fig. 4. Deformation mechanisms of the CoCrFeNiB0.3 matrix and dendrite during the micro-cantilever-bending tests. (a) Bright field image of the CoCrFeNiB0.3 matrix with a selected area electron diffraction pattern as the inset image, showing many deformation twins. (b) Interaction between the deformation twins and the stacking faults in the CoCrFeNiB0.3 matrix. (c) Bright-field image of the CoCrFeNiB0.3 dendrite. (d) Interaction between the dislocations and precipitates in the CoCrFeNiB0.3 dendrite.

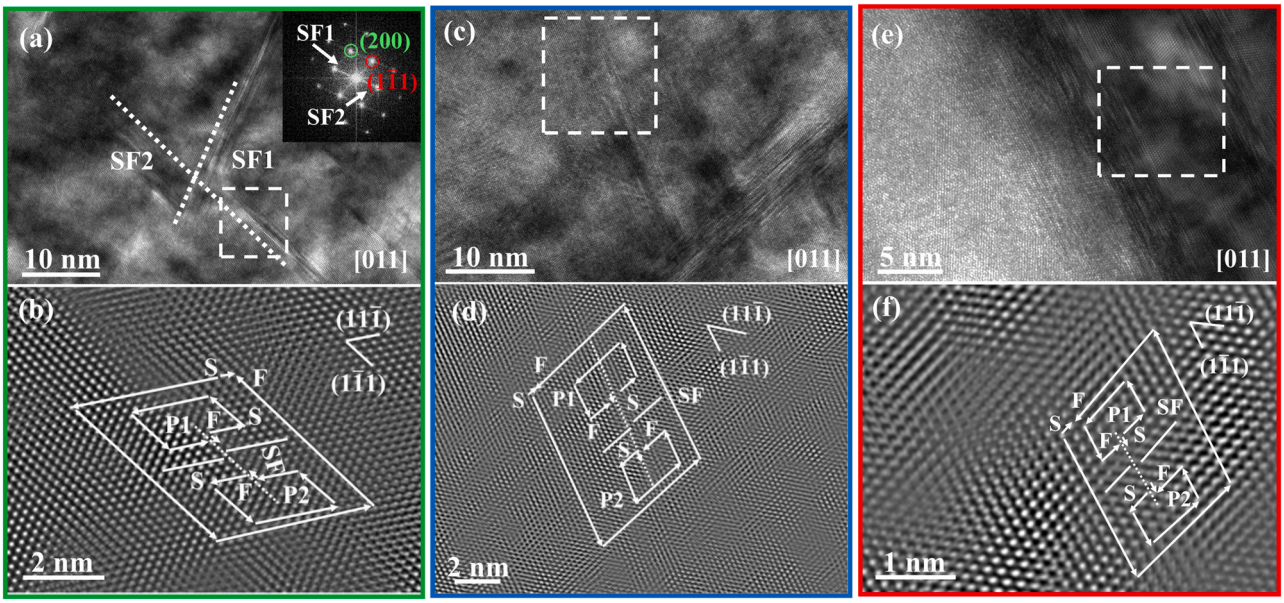

Fig. 5. HRTEM image and the corresponding IFFT image with Burgers circuits surrounding the entire SF. (a-b) CoCrFeNi HEA. (c-d) CoCrFeNiB0.3 matrix. (e-f) CoCrFeNiB0.3 dendrite.

phenomena have been found in other HEAs with an FCC structure [37–41].

Compared with the CoCrFeNi HEA, the deformation twins of the CoCrFeNiB0.3 matrix increased significantly, indicating that the dominant deformation mechanism is the deformation twins (Fig. 4). Yamakov et al. found that the twinning ability increased with the decrease of SFE. Alloys with lower SFE have a better deformation twining ability [42]. In this study, the SFE of the CoCrFeNiB0.3 matrix was obviously lower than that of the CoCrFeNi HEA. Regarding the specific reasons for the decrease of SFE in alloys, Mishra et.al claimed that the high lattice distortion might decrease the SFE [43]. According to the X-ray diffraction (XRD) results (see the Supplementary Materials for more details), the solid solution of boron in the matrix increased the lattice distortion, thus reducing the SFE in the CoCrFeNiB0.3 matrix. In terms of the effect of boron on the SFE of alloys, Shi et al. found that the trace boron doping could lead to the decrease of the SFE in CoCrNi alloys, thereby generating more SFs as new embryos within the deformation twins with increasing the strain [44].

When boron existed in the form of borides, the dominant deformation mechanism transformed from deformation twins to dislocation slip (Fig. 4), which was mainly attributed to the increase of SFE (Fig. 5). Similarly, according to the SF width in Fig. 5, it can be found that the SFE of the CoCrFeNiB0.3 dendrite was higher than that of the CoCrFeNi HEA, which indicates that the formation of large numbers of borides can increase the SFE. According to the experimental results and density functional theory (DFT) calculations, Ni has a very high SFE of ~150 mJ/m^2 [45]. Adding Co, Cr, or Fe to Ni can decrease its SFE. Cr has the strongest effect on SFE, followed by Co, and Fe presents the weakest effect [45]. For the current CoCrFeNi HEA, Ni was regarded as a solvent. Thus, the SFE of CoCrFeNi HEA was ~30 mJ/m^2 [36]. According to the differences in the chemical compositions of Cr in the CoCrFeNi HEA and CoCrFeNiB0.3 dendrite listed in Table 1, the loss of Cr in the matrix, accompanied by the formation of Cr_2B, led to a relatively-higher SFE of the CoCrFeNiB0.3 dendrite than the CoCrFeNi HEA. The increase of the SFE inhibited the formation of the deformation twins and promoted the rate of dislocation cross-slip or climb. When the dislocations encountered the borides during slip, dislocation accumulation occurred near the borides (Fig. 4).

4. Conclusion

In summary, the present work demonstrates that the existing form of boron has a significant effect on the deformation mechanism of the FCC HEAs by varying the SFE. The dominant deformation mechanism of CoCrFeNi HEAs is dislocation slip. When boron atoms were interstitials of solid solutions, large lattice distortion was produced, reducing the SFE of CoCrFeNi HEAs, thereby leading to the transformation of the deformation mechanism from dislocation slip to deformation twins. When Cr_2B was formed, Cr_2B reduced the content of Cr in the matrix, thus increasing the SFE of the matrix and resulting in the transformation of deformation mechanism from the deformation twin to dislocation slip. These discoveries may tune the deformation mechanism of FCC HEAs via interstitial atom doping, as well as provides new insights for designing HEAs.

CRediT authorship contribution statement

Haitao Zhang: Methodology, Data curation, Writing – original draft preparation. **Chenglin Wang:** Software and Writing – reviewing and editing. **Shuyan Shi:** processing the micro-cantilever beams and TEM samples. **Yiping Lu:** Writing – reviewing and editing, Visualization, Supervision. **Tingju Li:** Writing – reviewing and editing, Supervision. **Longjiang Zou:** Writing – reviewing and editing. **Peter K. Liaw:** Writing – reviewing and editing.

Declaration of Competing Interest

The authors declare that they have no known competing financial interests or personal relationships that could have appeared to influence the work reported in this paper.

Acknowledgments

This work was supported by the National Natural Science Foundation of China (Nos. 51822402 and U20A20278), the National Key Research and Development Program of China (Nos. 2019YFA0209901 and 2018YFA0702901), the fund of the State Key Laboratory of Solidification Processing in NWPU (No. SKLSP201902)

and the Liao Ning Revitalization Talents Program (No. XLYC1807047). P. K. Liaw appreciates support from the National Science Foundation (DMR-1611180 and 1809640) and the US Army Research Office (W911NF-13-1-0438 and W911NF-19-2-0049).

References

[1] J.W. Yeh, S.K. Chen, S.J. Lin, J.Y. Gan, T.S. Chin, T.T. Shun, C.H. Tsau, S.Y. Chang, Nanostructured high-entropy alloys with multiple principal elements: novel alloy design concepts and outcomes, Adv. Eng. Mater. 6 (2004) 299–303.
[2] B. Cantor, I.T.H. Chang, P. Knight, A.J.B. Vincent, Microstructural development in equiatomic multicomponent alloys, Mater. Sci. Eng.: A, 375 377 (2004) 213–218.
[3] Y. Zhang, T.T. Zuo, Z. Tang, M.C. Gao, K.A. Dahmen, P.K. Liaw, Z.P. Lu, Microstructures and properties of high-entropy alloys, Prog. Mater. Sci. 61 (2014) 1–93.
[4] X. Yang, Y. Zhang, Prediction of high-entropy stabilized solid-solution in multi-component alloys, Mater. Chem. Phys. 132 (2012) 233–238.
[5] Y. Zhang, Y.J. Zhou, J.P. Lin, G.L. Chen, P.K. Liaw, Solid-solution phase formation rules for multi-component alloys, Adv. Eng. Mater. 10 (2008) 534–538.
[6] H. Zheng, R. Chen, G. Qin, X. Li, Y. Su, H. Ding, J. Guo, H. Fu, Transition of solid-liquid interface and tensile properties of CoCrFeNi high-entropy alloys during directional solidification, J. Alloy. Compd. 787 (2019) 1023–1031.
[7] W.H. Liu, Z.P. Lu, J.Y. He, J.H. Luan, Z.J. Wang, B. Liu, Y. Liu, M.W. Chen, C.T. Liu, Ductile CoCrFeNiMox high entropy alloys strengthened by hard intermetallic phases, Acta Mater. 116 (2016) 332–342.
[8] T. Shun, L. Chang, M. Shiu, Microstructures and mechanical properties of multiprincipal component CoCrFeNiTix alloys, Mater. Sci. Eng.: A 556 (2012) 170–174.
[9] H. Jiang, K. Han, D. Qiao, Y. Lu, Z. Cao, T. Li, Effects of Ta addition on the microstructures and mechanical properties of CoCrFeNi high entropy alloy, Mater. Chem. Phys. 210 (2018) 43–48.
[10] F. He, Z. Wang, X. Shang, C. Leng, J. Li, J. Wang, Stability of lamellar structures in CoCrFeNiNbx eutectic high entropy alloys at elevated temperatures, Mater. Des. 104 (2016) 259–264.
[11] Z. Lei, X. Liu, Y. Wu, H. Wang, S. Jiang, S. Wang, X. Hui, Y. Wu, B. Gault, P. Kontis, D. Raabe, L. Gu, Q. Zhang, H. Chen, H. Wang, J. Liu, K. An, Q. Zeng, T. Nieh, Z. Lu, Enhanced strength and ductility in a high-entropy alloy via ordered oxygen complexes, Nature 563 (2018) 546–550.
[12] J. Li, B. Gao, Y. Wang, X. Chen, Y. Xin, S. Tang, B. Liu, Y. Liu, M. Song, Microstructures and mechanical properties of nano carbides reinforced CoCrFeMnNi high entropy alloys, J. Alloy. Compd. 792 (2019) 170–179.
[13] Z. Wang, I. Baker, Z. Cai, S. Chen, J.D. Poplawsky, W. Guo, The effect of interstitial carbon on the mechanical properties and dislocation substructure evolution in Fe40.4Ni11.3Mn34.8Al7.5Cr6 high entropy alloys, Acta Mater. 120 (2016) 228–239.
[14] Z. He, N. Jia, H. Yan, Y. Shen, M. Zhu, X. Guan, X. Zhao, S. Jin, G. Sha, Y. Zhu, C.T. Liu, Multi-heterostructure and mechanical properties of N-doped FeMnCoCr high entropy alloy, Int. J. Plast. 139 (2021) 102965.
[15] Q. Yu, L. Qi, T. Tsuru, R. Traylor, D. Rugg, J.W. Morris, M. Asta, D.C. Chrzan, A.M. Minor, Origin of dramatic oxygen solute strengthening effect in titanium, Science 347 (2015) 635–639.
[16] Z. Wang, I. Baker, Interstitial strengthening of a f.c.c, FeNiMnAlCr High. entropy Alloy, Mater. Lett. 180 (2016) 153–156.
[17] I. Moravcik, H. Hadraba, L. Li, I. Dlouhy, D. Raabe, Z. Li, Yield strength increase of a CoCrNi medium entropy alloy by interstitial nitrogen doping at maintained ductility, Scr. Mater. 178 (2020) 391–397.
[18] J. Pang, H. Zhang, L. Zhang, Z. Zhu, H. Fu, H. Li, A. Wang, Z. Li, H. Zhang, Simultaneous enhancement of strength and ductility of body-centered cubic TiZrNb multi-principal element alloys via boron-doping, J. Mater. Sci. Technol. 78 (2021) 74–80.
[19] M.P. Seah, Adsorption-induced interface decohesion, Acta Metall. 28 (1980) 955–962.
[20] C.T. Liu, C.L. White, J.A. Horton, Effect of boron on grain-boundaries in Ni3Al†, Acta Metall. 33 (1985) 213–229.
[21] J.B. Seol, J.W. Bae, Z. Li, J. Chan Han, J.G. Kim, D. Raabe, H.S. Kim, Boron doped ultrastrong and ductile high-entropy alloys, Acta Mater. 151 (2018) 366–376.
[22] Q. CHEN, Y. LU, Y. DONG, T. WANG, T. LI, Effect of minor B addition on microstructure and properties of AlCoCrFeNi multi-compenent alloy, Trans. Nonferrous Met. Soc. China 25 (2015) 2958–2964.
[23] L. Tang, K. Yan, B. Cai, Y. Wang, B. Liu, S. Kabra, M.M. Attallah, Y. Liu, Deformation mechanisms of FeCoCrNiMo0.2 high entropy alloy at 77 and 15 K, Scr. Mater. 178 (2020) 166–170.
[24] R. Ding, J. Gong, A.J. Wilkinson, I.P. Jones, < c+a > Dislocations in deformed Ti–6Al–4V micro-cantilevers, Acta Mater. 76 (2014) 127–134.
[25] Y. Zou, P. Okle, H. Yu, T. Sumigawa, T. Kitamura, S. Maiti, W. Steurer, R. Spolenak, Fracture properties of a refractory high-entropy alloy: In situ micro-cantilever and atom probe tomography studies, Scr. Mater. 128 (2017) 95–99.
[26] Jicheng, Gong, T., Benjamin, Britton, Mitchell, A., Cuddihy, Fionn, E. P., < a > Prismatic, < a > basal, and < c+a > slip strengths of commercially pure Zr by micro-cantilever tests, Acta Materialia, (2015).
[27] R. Ding, J. Gong, A.J. Wilkinson, I.P. Jones, A study of dislocation transmission through a grain boundary in hcp Ti–6Al using micro-cantilevers, ACTA MATERIALIA (2016).
[28] C. Wang, S. Shi, Y. Deng, P. Gai, G. Chen, X. Fu, W. Zhou, Friction control by tailoring deformation mechanism of interfacial grains in metals, Mater. Sci. Eng.: A 828 (2021) 142105.
[29] Z. Yan, Y. Lin, On the widths of stacking faults formed by dissociation of different types of full dislocations in a nanostructured Al alloy, Mater. Sci. Eng.: A 770 (2020) 138532.
[30] H. Ma, C.H. Shek, Effects of Hf on the microstructure and mechanical properties of CoCrFeNi high entropy alloy, J. Alloy. Compd. 827 (2020) 154159.
[31] Wong-Ng Winnie, F. Howard, Boris McMurdie, Camden Paretzkin, Hubbard R, Standard X-ray diffraction powder patterns of fifteen ceramic phases, Powder Diffr. 2 (1987) 106–117.
[32] G. Jicheng, Anisotropy in the plastic flow properties of single-crystal alpha-Titamium, Acta Mater. 57 (19) (2009) 5693–5705.
[33] J. He, Q. Wang, H. Zhang, L. Dai, T. Mukai, Y. Wu, X. Liu, H. Wang, T. Nieh, Z. Lu, Dynamic deformation behavior of a face-centered cubic FeCoNiCrMn high-entropy alloy, Sci. Bull. 63 (2018) 362–368.
[34] H. Idrissi, K. Renard, L. Ryelandt, D. Schryvers, P.J. Jacques, On the mechanism of twin formation in Fe–Mn–C TWIP steels, Acta Mater. 58 (2010) 2464–2476.
[35] A.H. Cottrell, Theory of dislocations, Prog. Met. Phys. 4 (1953) 205–264.
[36] R. Mayahi, A theoretical investigation on deformation behavior and phase prediction of CoCrFeNi-based high entropy alloys, Materials Today, Communications 24 (2020) 101025.
[37] Y. Zhang, T.T. Zuo, Z. Tang, M.C. Gao, K.A. Dahmen, P.K. Liaw, Z.P. Lu, Microstructures and properties of high-entropy alloys, Prog. Mater. Sci. 61 (2014) 1–93.
[38] A.J. Zaddach, C. Niu, C.C. Koch, D.L. Irving, Mechanical properties and stacking fault energies of NiFeCrCoMn high-entropy alloy, JOM 65 (2013) 1780–1789.
[39] Z. Zhang, M.M. Mao, J. Wang, B. Gludovatz, Z. Zhang, S.X. Mao, E.P. George, Q. Yu, R.O. Ritchie, Nanoscale origins of the damage tolerance of the high-entropy alloy CrMnFeCoNi, Nature, Communications 6 (2015).
[40] F. Otto, A. Dlouhý, C. Somsen, H. Bei, G. Eggeler, E.P. George, The influences of temperature and microstructure on the tensile properties of a CoCrFeMnNi high-entropy alloy, Acta Mater. 61 (2013) 5743–5755.
[41] D. Choudhuri, M. Komarasamy, V. Ageh, R.S. Mishra, Investigation of plastic deformation modes in Al0.1CoCrFeNi high entropy alloy, Mater. Chem. Phys. 217 (2018) 308–314.
[42] V. Yamakov, D. Wolf, S.R. Phillpot, A.K. Mukherjee, H. Gleiter, Deformation-mechanism map for nanocrystalline metals by molecular-dynamics simulation, Nat. Mater. 3 (2004) 43–47.
[43] R.S. Mishra, N. Kumar, M. Komarasamy, Lattice strain framework for plastic deformation in complex concentrated alloys including high entropy alloys, Mater. Sci. Technol. 31 (2015) 1259–1263.
[44] Y. Shi, Y.D. Wang, S. Li, R. Li, Y. Wang, Mechanical behavior in boron-microalloyed CoCrNi medium-entropy alloy studied by in situ high-energy X-ray diffraction, Materials Science and Engineering: A, 788.
[45] P.C.J. Gallagher, The influence of alloying, temperature, and related effects on the stacking fault energy, Metall. Trans. 1 (1970) 2429–2461.